IV. Discussion

CBED [001] zone-axis patterns from thin crystals of this preparation are consistent with a stacking-faulted form of the hexagonal, $P6_3/mmc$, GaS structure, following the model found by Johnson (1972) for graphite. These patterns are, however, insensitive to the detailed host-lattice structure. High-resolution lattice images obtained from the [110] orientation provide the required complementary data. These images appear to be consistent only with a host lattice which has the HP-type stacking.

The crystal sizes and thicknesses of the CBED samples were much less than those used in the electron microscopy; however, the high density of stacking faults observed in both investigations suggests that faulting is a property of the bulk preparation, and contrasts with all reported observations made on well annealed β-GaS.

In the β phase, neighbouring kinked layers are matched geometrically, a feature which has been put forward as a principal reason for a disinclination for stacking faulting (Basinsky, Dove & Mooser, 1963). Such matching does not occur in the HP structure. If the latter were present in the preparation at room pressure and temperature, transformation to the β phase by means of stacking faulting would become energetically favoured, resulting in a reduction of the volume of HP phase present to small islands, metastably held by surrounding dislocations and stacking faults.

From our combined convergent-beam diffraction and high-resolution microscopy analysis we conclude that GaS annealed below 973 K still contains a proportion of HP-GaS in metastable form, interspersed with stacking faults.

This observation would explain the low stacking-fault energy associated with this sample, and should help to explain apparently conflicting conclusions drawn in the past concerning the structure of GaS, when a variety of preparation and annealing techniques have been used.

References

D'AMOUR, H., HOLZAPFEL, W. B., POLIAN, A. & CHEVY, A. (1982). *Solid State Commun.* **44**, 853-855.

BASINSKY, Z. S., DOVE, D. B. & MOOSER, E. (1963). *J. Appl. Phys.* **34**, 469-468.

BASTOW, T. F., CAMPBELL, I. D. & WHITFIELD, H. J. (1981). *Solid State Commun.* **39**, 307-311.

GARD, F. A. (1966). *Nature (London)*, **211**, 1078-1079.

GOODMAN, P. & WHITFIELD, H. J. (1980). *Acta Cryst.* A**36**, 219-228.

JOHNSON, A. W. S. (1968). *Acta Cryst.* A**24**, 534-543.

JOHNSON, A. W. S. (1972). *Acta Cryst.* A**28**, 89-91.

KUHN, A. & CHEVY, A. (1976). *Acta Cryst.* B**32**, 983-984.

KUHN, A., CHEVY, A. & CHEVALIER, R. (1975). *Phys. Status Solidi A*, **31**, 469-475.

MOODIE, A. F. & WHITFIELD, H. J. (1983). *Acta Cryst.* A**39**, 946-947.

SCHUBERT, K., DÖRRE, E. & KLUGE, M. (1955). *Acta Metall.* **46**, 216-224.

WYCKOFF, W. G. (1963). *Crystal Structures* Vol. 1, pp. 144-145. New York: Interscience.

ZEIL, J. P. VAN DER, MEIXNER, A. E. & KASPER, H. M. (1973). *Solid State Commun.* **12**, 1213-1215.

Acta Cryst. (1985). B**41**, 298-304

The Anharmonic Thermal Vibration in ZnX (X = S, Se, Te) and Its Dependence on the Chemical-Bond Characters

BY TAKAMITSU YAMANAKA AND MASAYASU TOKONAMI

Mineralogical Institute, Faculty of Science, University of Tokyo, Hongo, Tokyo 113, *Japan*

(*Received* 20 *February* 1985; *accepted* 22 *April* 1985)

Abstract

The X-ray diffraction study of anharmonic thermal vibration was carried out with respect to ZnX (X = S, Se, Te), having a zinc-blende structure, whose lattice-dynamical properties such as force constant and effective charge were determined by Raman spectroscopy. Difference Fourier syntheses based on harmonic refinements after correction of the diffraction intensities for thermal diffuse scattering exhibit a tetrapod shape of residual electron density around the Zn atoms, implying an anisotropy of the anharmonic thermal vibration. However, the residual density around the X atoms was subjected to influences of both the valence charge electrons and the anharmonic thermal vibration of the atoms. ZnTe, having a smaller interatomic force constant and less ionic bond character than ZnS and ZnSe, showed the most remarkable anharmonicity among the three compounds. The difference Fourier syntheses of ZnTe showed that the higher-order reflections indicated more salient anharmonicity and that the Zn atom has a larger anharmonic vibration than the Te atom. Cumulant expansion up to the fourth-rank tensors

0108-7681/85/050298-07$01.50

was applied to the temperature factors in the anharmonic refinement. One-particle potentials of the three samples along the directions [111], [110] and [100] were evaluated from the anharmonic temperature factors. These potential maps interpret well the residual electron distribution found in the difference Fourier maps obtained from the harmonic refinements.

Introduction

A number of studies on the anharmonic thermal vibration of atoms in crystals have been made by means of neutron diffraction, which may overcome the difficulties caused by the simultaneous presence of both anharmonic thermal motion and aspherical valence charge density. The contribution of the anharmonic components to X-ray diffraction intensities has also been investigated and the experimental capability of the analysis has been proved.

The empirical derivations of the probability density function (p.d.f.) or one-particle potential (OPP) with respect to the anharmonicity have been proposed by using the multimodule distribution functions: Edgeworth expansion, Gram–Charlier expansion and Taylor expansion. Moss, McMullan & Koetzle (1980), Zucker & Schulz (1982) and Kuhs (1983) tested these functions and proposed the best proper model for the atomic thermal motion.

In order to understand the nature of anharmonic thermal motion, other than the thermal variation of the anharmonic motion, we studied the effect of the chemical-bond character on the anharmonicity. X-ray diffraction experiments were made with respect to ZnX (X = S, Se, Te), all having a zinc-blende structure ($F\bar{4}3m$; $Z=4$; Zn on $\bar{4}3m$ at 0, 0, 0 and X on $\bar{4}3m$ at $\frac{1}{4}$, $\frac{1}{4}$, $\frac{1}{4}$) but different bond characters. The anharmonic thermal vibration of the atoms was represented by the refinement of the thermal parameters based on the cumulant expansion and one-particle potentials, together with the difference Fourier syntheses.

The Zn–X bond nature was characterized by the calculation of the lattice-dynamical properties of effective charge Z_e(Zn) and force constant K(Zn$\cdots X$) on the basis of the Raman spectra.

Discussions on the anharmonicity of a series of compounds are also made in comparison with the previously reported neutron diffraction studies of ZnS and ZnTe by Cooper, Rouse & Fuess (1973) and of ZnS by Moss *et al.* (1980) and the X-ray study of ZnS by McIntyre, Moss & Barnea (1980).

Experimental

Single crystals of ZnS, ZnSe and ZnTe having the zinc-blende structure were prepared by the method of vapour growth in an evacuated silica-glass tube at 1073 K. The crystals grown were ground to a sphere with a diameter of about 200–300 μm. A spherical test piece of each sample having neither twins nor a mixture of the wurtzite structure derived from the stacking faults of layers was selected by means of precession photography. Cell dimensions of the three samples were determined by the least-squares procedure applying the 2θ values of 25 independent reflections falling within the range $40°<2\theta<50°$ measured by single-crystal diffractometry. Accurate measurement of the X-ray diffraction intensities at room temperature was made on a Rigaku AFC5 four-circle diffractometer set on the rotating-anode X-ray generator (160 mA, 50 kV) using graphite-monochromated Mo $K\alpha$ radiation ($\lambda=0{\cdot}71069$ Å). The integrated intensities were collected under the following conditions: (1) ω–2θ scanning in the bisecting mode; (2) scanning speed $6°\,\text{min}^{-1}$ in 2θ; (3) scan width $1{\cdot}5°+0{\cdot}45°\tan\theta$ in 2θ. Reflections with $|I_o|>3\sigma|I_o|$ collected within $0{\cdot}1\,\text{Å}^{-1}<\sin\theta/\lambda<1{\cdot}32\,\text{Å}^{-1}$ were used for the refinement.

Table 1. *Elastic constants* (GPa) *at* 293 K

	c_{11}	c_{44}	c_{12}	Reference
ZnS	98·5	44·8	63·0	Vekilov & Rusakov (1971)
ZnSe	90·0	40·0	55·0	Kuskov *et al.* (1972)
ZnTe	71·5	31·4	40·8	Lee (1970)

Before the refinement, the correction of the thermal diffuse scattering (TDS) for the integrated intensities was made by adopting a model of first-order scattering due to one-phonon acoustic lattice vibration. Correction was carried out in terms not only of elastic constants but also of scanning modes and scanning vector defined by the UB matrix (Busing & Levy, 1967). The three independent elastic constants c_{11}, c_{44} and c_{12} of ZnX were taken from Vekilov & Rusakov (1971) for ZnS, from Kuskov, Rusakov & Mentser (1972) for ZnSe and from Lee (1970) for ZnTe (Table 1). The program *SXTD*1 (Merisalo & Kurittu, 1978) was used for the evaluation of the TDS correction factor α in the equation: $I_o=I_{\text{Bragg}}(1+\alpha)$. The TDS correction was detailed in our previous paper (Yamanaka, Takeuchi & Tokonami, 1984). Corrections of the diffraction intensities were made for the Lorentz factor, polarization and absorption [μr(ZnS) = 1·65, μr(ZnSe) = 2·95, μr(ZnTe) = 2·67].

Harmonic refinement and difference Fourier synthesis

The refinement of the three compounds ZnX (X = S, Se, Te) based on the harmonic oscillation model was initiated by the ordinary full-matrix least-squares procedure. In the refinement, atomic scattering factors of neutral atoms were adopted for the least-squares calculation. Only the temperature factors were variable parameters. An isotropic-extinction parameter G_{ext} was also calculated by the type I model (Becker & Coppens, 1974). The final reliability factors $R[=\sum(\|F_o|-|F_c\|)/\sum|F_c|]$ of the refinements of ZnS,

Table 2. *Harmonic and anharmonic thermal parameters*

		ZnS			ZnSe			ZnTe		
	a (Å)	5·4053			5·6609			6·0862		
	$\sin\theta/\lambda$ (Å^{-1})	1·32			1·32			1·32		
	No. of reflections	107			93			142		
		Harm		Anharm.	Harm		Anharm.	Harm		Anharm.
		—	TDS	TDS	—	TDS	TDS	—	TDS	TDS
	R(%)	1·74	1·66	1·29	1·68	1·68	1·60	1·63	1·58	1·54
	wR(%)	1·78	1·72	1·32	1·62	1·62	1·61	1·63	1·51	1·54
Zn	$\beta_{11}\times10^5$	749 (7)	758 (6)	746 (6)	877 (12)	882 (12)	870 (9)	897 (9)	899 (8)	893 (6)
	$\gamma_{123}\times10^7$			320 (9)			932 (10)			1289 (17)
	$\delta_{1111}\times10^8$			90 (9)			487 (10)			270 (15)
	$\delta_{1122}\times10^8$			−85 (6)			307 (6)			200 (6)
X	$\beta_{11}\times10^5$	600 (10)	613 (10)	610 (8)	593 (7)	597 (7)	567 (4)	619 (4)	622 (4)	651 (5)
	$\gamma_{123}\times10^7$			−258 (11)			−630 (15)			−892 (20)
	$\delta_{1111}\times10^8$			−437 (10)			−435 (12)			−150 (17)
	$\delta_{1122}\times10^8$			−87 (9)			−124 (10)			−166 (13)
	$G_{ext}\times10^6$	6·88	6·88	7·13	8·72	8·72	8·78	3·00	3·00	3·10

Table 3. *Harmonic refinement of* ZnTe *as a function of* $\sin\theta/\lambda$

$T=\sin\theta/\lambda$ (Å^{-1})	$0<T\le0.7$	$0<T\le0.9$	$0<T\le1.32$	$0.7\le T\le1.32$	$0.8\le T\le1.32$	$0.9\le T\le1.32$
No. of reflections	31	56	139	111	99	83
R(%)	0·40	0·79	1·58	2·88	3·11	3·41
wR(%)	0·52	0·94	1·51	3·20	3·53	4·05
β_{11}(Zn)$\times10^5$	910 (11)	900 (8)	899 (9)	892 (13)	898 (16)	897 (24)
β_{11}(Te)$\times10^5$	631 (9)	627 (7)	622 (4)	619 (13)	621 (17)	624 (28)
B(Zn) (Å^2)	1·35	1·34	1·33	1·32	1·33	1·33
B(Te) (Å^2)	0·94	0·93	0·92	0·92	0·92	0·97
$G_{ext}\times10^6$	3·23	3·17	3·10	6·94	8·84	54·4

ZnSe and ZnTe are 0·017, 0·0168 and 0·0163, respectively. The results of the refinements and the experimental conditions are presented in Table 2.* The thermal parameters of the Zn atom in the three samples are larger than those of the X atoms. This accords well with the neutron diffraction studies (Cooper *et al.*, 1973; Moss *et al.*, 1980).

In spite of the fact that both atoms Zn and X have the same site symmetry, the Zn atom with a smaller atomic radius has a larger harmonic thermal parameter β_{11} than all the X atoms in the three samples. The difference between β_{11}(Zn) and $\beta_{11}(X)$ is largest in ZnTe. It may possibly be concluded that these parameters are related to the reduced mass of Zn and X and their atomic radii.

The diffraction intensities of the higher-order reflections are less affected by the valence electrons. Hence, the refinement based on these reflections must be significant in order to elucidate the atomic thermal vibration. This phenomenon was assured by the refinements of ZnTe based on the higher-order reflections falling within the range $r_1<\sin\theta/\lambda<1{\cdot}32$ Å^{-1} ($r_1=0{\cdot}7$, 0·8, 0·9 Å^{-1}) and $0<\sin\theta/\lambda<r_2$ ($r_2=0{\cdot}7$, 0·9, 1·32 Å^{-1}) in Table 3.

Difference Fourier syntheses were carried out after the harmonic refinements of ZnS, ZnSe and ZnTe. The difference Fourier map in the (110) plane including Zn and X atoms (Fig. 1) exhibits residual electron densities around Zn and X (= S, Se, Te) atoms. The positive and negative residual peaks around Zn show a tetrapod shape of electron density distribution. No split atoms are visible in the difference Fourier maps. An aspherical electron distribution is not expected because of the electron configuration of Zn ($3d^{10}4s^2$). Hence, the residue around Zn is expected to result mainly from the anharmonic atomic thermal vibration.

Despite the fact that the X (=S, Se, Te) atom has the same site symmetry as Zn, the residue around X in the difference Fourier maps is not similar to that around Zn. The former is characterized by the localization of the valence electrons and anharmonic thermal vibrations of the X atoms. The valence charge density distribution disregarding thermal motion was theoretically calculated by Cohen (1973) using the empirical pseudopotential: $V(\mathbf{r})=\sum V(Q)F(Q)\exp(i\mathbf{Q}\mathbf{r})$, where $F(Q)$ and $V(Q)$ are the structure factor and pseudopotential form factor, respectively. The calculation reveals that the valence charge density in ZnSe is localized only around Se atoms. Consequently, the residue around the Zn atoms may possibly be regarded as the aspherical electron distribution mainly caused by the atomic thermal motion. In order to discuss quantitatively the

* Lists of structure factors have been deposited with the British Library Lending Division as Supplementary Publication No. SUP 42189 (4 pp.). Copies may be obtained through The Executive Secretary, International Union of Crystallography, 5 Abbey Square, Chester CH1 2HU, England.

anharmonicity of ZnX, reference will be made only to Zn atoms in the later calculation of the one-particle potential (OPP).

The difference Fourier maps of ZnTe based on the reflections in the various diffraction ranges, $r_1 < \sin\theta/\lambda < r_2$, are shown in Fig. 2. These maps show that a more distinct indication of the anharmonicity is given in the higher-order reflections. The difference Fourier syntheses obtained from the reflections with $0{\cdot}9\ \text{Å}^{-1} < \sin\theta/\lambda < 1{\cdot}32\ \text{Å}^{-1}$ shown in Fig. 3 are characterized mainly by the anharmonic thermal atomic vibrations. Therefore, the residual electron densities around the Te atoms which appeared in Fig. 1, which are probably due to the aspherical valence electron distribution, are almost absent in Fig. 3. The residual electron densities which are more salient around Zn than around Te may suggest that the anharmonicity of Zn is predominant over that of X(=S, Se, Te). Features in Fig. 3 are in accordance with those of the difference Fourier map obtained from the neutron diffraction study of ZnS by Moss *et al.* (1980).

Lattice-dynamical calculation

The aforementioned harmonic refinements were carried out on the assumption that all atoms were not ionized but neutral. The succeeding difference Fourier syntheses reveal that ZnTe is characterized by more noticeable anharmonicity than ZnS and ZnSe. The difference in the anharmonicity is related to such lattice-dynamical properties as the force constant and the effective charge. Cowley (1963) initiated the lattice-dynamical theory of the anharmonic thermal vibration in a crystal by means of the Grüneisen parameter and demonstrated a quasiharmonic model of the anharmonicity. The Grüneisen parameter is calculated in terms of the lattice frequency shift observed from Raman spectroscopy.

For the present lattice-dynamical calculation, the transverse (ν_{TO}) and longitudinal (ν_{LO}) optical wavenumbers of ZnX (X = S, Se, Te) were measured by the Ar-laser Raman spectrometer (JASCO R-500) at high temperatures and at pressure. ZnX with point symmetry $\bar{4}3m$ has only one Raman-active mode F_2. A number of measurements of the lattice vibrations of these samples at room temperature have been reported and they are summarized by Wilkinson (1973).

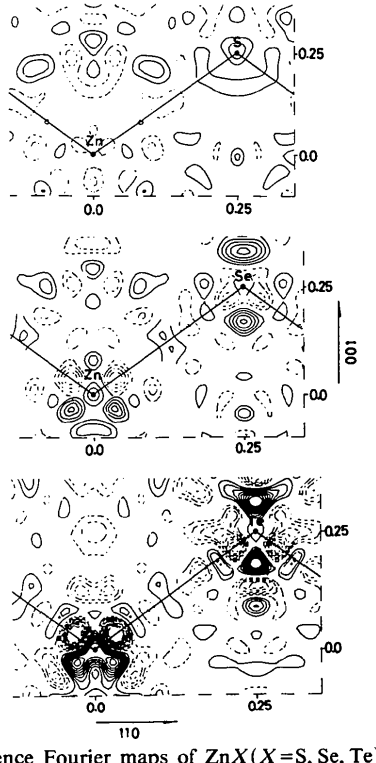

Fig. 1. Difference Fourier maps of ZnX(X=S, Se, Te) from the harmonic refinements in the $(1\bar{1}0)$ plane, passing through the Zn and X atoms; top ZnS, middle ZnSe and bottom ZnTe. Solid and broken lines represent positive and negative contours, respectively. A contour indicating zero is omitted. Contours are drawn at intervals of $0{\cdot}2\ \text{e Å}^{-3}$.

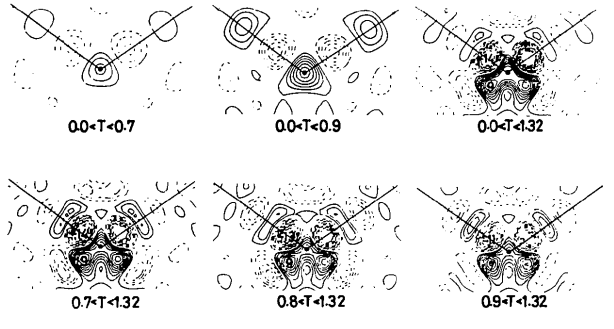

Fig. 2. Residual electron density around the Zn atom observed in the difference Fourier maps of ZnTe based on the reflections falling within the various diffraction ranges. The term T denotes the value of $\sin\theta/\lambda$ (Å^{-1}) The Fourier section and contour interval are as in Fig. 1.

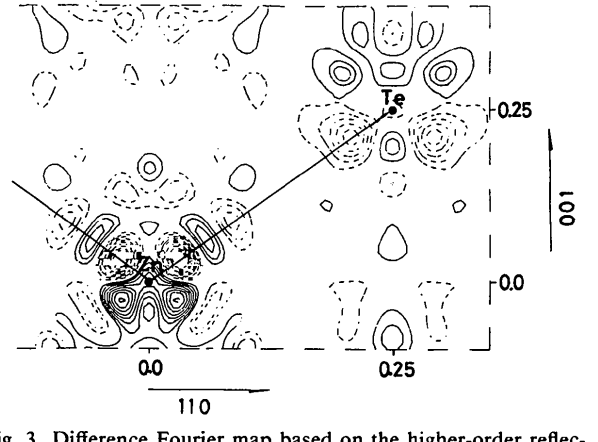

Fig. 3. Difference Fourier map based on the higher-order reflections of ZnTe falling in the range $0{\cdot}9 < \sin\theta/\lambda < 1{\cdot}32\ \text{Å}^{-1}$. The Fourier section and contour interval are as in Fig. 1.

The effective charge Z_e(Zn) and the interatomic force constant K(Zn···X) are evaluated by both the rigid-ion and the shell model (Kellermann, 1940; Dick & Overhauser, 1958). The calculations were made with the following equations:

(1) rigid-ion model

$$(2\pi\nu_{TO})^2 = (\beta/\mu) - 4\pi(Z_e)^2/3\mu V \quad (1)$$

$$(2\pi\nu_{LO})^2 = (\beta/\mu) + 8\pi(Z_e)^2/3\mu V \quad (2)$$

(2) shell model

$$(2\pi\nu_{TO})^2 = (\beta/\mu) - 4\pi(\varepsilon_\infty+2)(Z_e)^2/9\mu V \quad (3)$$

$$(2\pi\nu_{LO})^2 = (\beta/\mu) + 8\pi(\varepsilon_\infty+2)(Z_e)^2/9\mu V\varepsilon_\infty, \quad (4)$$

where μ and V represent the reduced mass and volume of the unit cell and ε_∞ denotes a high-frequency dielectric constant (optical dielectric constant). In these equations, the first and second terms correspond to the short-range potential and to the long-range Coulomb potential, respectively. The short-range force constant K(Zn···X) and effective charge are represented by β and Z_e, respectively.

The detailed procedure of the evaluations as a function of pressure or temperature and the results will be described elsewhere (Yamanaka, 1985). The values of Z_e and K(Zn···X) evaluated for both models as well as the ν_{TO} and ν_{LO} observed at room temperature are presented in Table 4. The ratio R of the Coulomb term to the short-range term in equations (1) and (3) is also presented. These evaluations show that ZnTe has a smaller force constant and is less ionic than ZnS and ZnSe.

These lattice-dynamic properties are related to the compressibility and thermal-expansion coefficient of ZnX. From both results of the above calculation and the foregoing difference Fourier syntheses, we may conclude that the anharmonicity of such a compound bearing a less ionic and more metallic bond character as ZnTe with a larger electron conductivity becomes more distinct, in comparison with the ionic compound ZnS and that the lattice expands more easily, since the interatomic forces are weakened.

Table 4. *Effective charge and force constant*

	ZnS	ZnSe	ZnTe
d(Zn–X) (Å)	2·342	2·454	2·637
V (Å^3)	158·3	182·1	225·8
μ (g)	21·51	35·76	43·23
ν_{TO} (cm^{-1})	282	207	117
ν_{LO} (cm^{-1})	352	246	206
Rigid-ion model			
Z_e(Zn)	0·88	0·76	0·74
K(Zn···X)(×10^{-8}N Å^{-1})	0·597	0·513	0·446
R	0·157	0·121	0·106
Shell model			
ε	8·00	8·33	9·86
ε_∞	5·14	5·90	7·28
Z_e(Zn)	0·84	0·71	0·65
K(Zn···X)(×10^{-8}N Å^{-1})	0·709	0·590	0·509
R	0·291	0·236	0·216

Anharmonic refinement

Among various approaches to the anharmonic refinement, the present study adopted a formalism of a structure factor including anharmonic temperature parameters, by applying the cumulant expansion, which was proposed by Johnson (1969). The temperature factor $T(\mathbf{h})$ is

$$T(\mathbf{h}) = \exp[(i^2/2!)\sum\sum\beta_{jk}h_jh_k + (i^3/3!)\sum\sum\sum\gamma_{jkl}h_jh_kh_l + (i^4/4!)\sum\sum\sum\sum\delta_{jklm}h_jh_kh_lh_m], \quad (5)$$

where β_{jk}, γ_{jkl} and δ_{jklm} are the components in the second, third- and fourth-rank polar tensors, respectively. The temperature parameters higher than fourth rank were truncated in the present refinements. With respect to the cubic site symmetry $43m$, β_{11} ($=\beta_{22}=\beta_{33}$), γ_{123}, δ_{1111} ($=\delta_{2222}=\delta_{3333}$) and δ_{1122} ($=\delta_{1133}=\delta_{2233}$) are independent variables. These constraints on the tensor coefficients are referred to by Johnson & Levy (1974). The full-matrix least-squares refinements including the above variables were carried out by the computer program *RFINE*4 (Finger & Prince, 1975). The convergence of the terms of γ_{123}(Zn) and $\gamma_{123}(X)$ in the least-squares procedure hardly succeeded because of their strong correlation, which prevented simultaneous refinement of these parameters. The following approximation was then adopted for their constraint in the least-squares calculation: $\gamma_{123}(X) = -\gamma_{123}(\mathrm{Zn}) \times \beta_{11}(X)_h/\beta_{11}(\mathrm{Zn})_h$, where $\beta_{11}(\mathrm{Zn})_h$ and $\beta_{11}(X)_h$ represent the harmonic temperature factors of the Zn and X atoms, respectively. The refinement reduced the R factor farther than the regular refinement of the harmonic thermal parameters. Hence, the former refinement was confirmed to be a more reliable analysis than the latter.

The anharmonic refinements of ZnX (Table 2) show a remarkably large value for γ_{123} of ZnTe, corresponding to a tetrapod shape of electron density. On the other hand, the term for ZnS has a very small value, indicating that it has only a slight anharmonicity in the atomic thermal vibration, compared with ZnTe. The above facts accord well with the features found in the difference Fourier maps (Fig. 1).

After the anharmonic refinement of ZnTe, the difference Fourier map (Fig. 4) shows little residue around not only Zn but also Te atoms. Accordingly the refinement has ensured a reliable treatment for the anharmonic thermal vibrations of the atoms.

One-particle potential

The temperature factor $T(\mathbf{h})$ is the Fourier transform of the probability density function $P(\mathbf{u})$:

$$T(\mathbf{h}) = \int P(\mathbf{u})\exp(2\pi i\mathbf{hu})\mathrm{d}\mathbf{u}. \quad (6)$$

$P(\mathbf{u})$ is related to the effective one-particle potential (OPP) $V(\mathbf{u})$. The function is derived by Willis (1969):

$$P(\mathbf{u}) = \exp[-V(\mathbf{u})/k_BT]/\int\int\int \exp[-V \times(u_1u_2u_3)/k_BT]\,du_1\,du_2\,du_3, \quad (7)$$

where k_B is the Boltzmann constant. With the assumption that each atom independently vibrates within the range of the average potential defined by its neighbours, the anharmonic potential $V(\mathbf{u})$ is given for $\bar{4}3m$ site symmetry by

$$V(\mathbf{u}) = V_o + \tfrac{1}{2}\alpha U^2 + \beta u_1u_2u_3 + \gamma U^4 + \delta(u_1^4+u_2^4+u_3^4-\tfrac{3}{5}U^4), \quad (8)$$

where $U^2 = u_1^2+u_2^2+u_3^2$ and $U^4 = (u_1^2+u_2^2+u_3^2)^2$.

The formalism of OPP as a function of the anharmonic thermal parameters has been proposed by Willis (1969) and Mair & Wilkins (1976), and several others. Zucker & Schulz (1982), Kuhs (1983) and Kontio & Stevens (1982) proposed the OPP equation derived from the coefficients of the Edgeworth expansion or Gram–Charlier expansion related to the anharmonic parameters. In the present calculation of the anharmonic potential, the parameters α, β, γ, and δ in the OPP equation (8) were determined on the basis of the coefficients β_{jk}, γ_{jkl} and δ_{jklm} in the cumulant expansion equation (5). The potential parameters presented in Table 5 were evaluated from the β_{11}, γ_{123}, δ_{1111} and δ_{1122} of ZnX (Table 2) in accordance with Kontio & Stevens (1982).

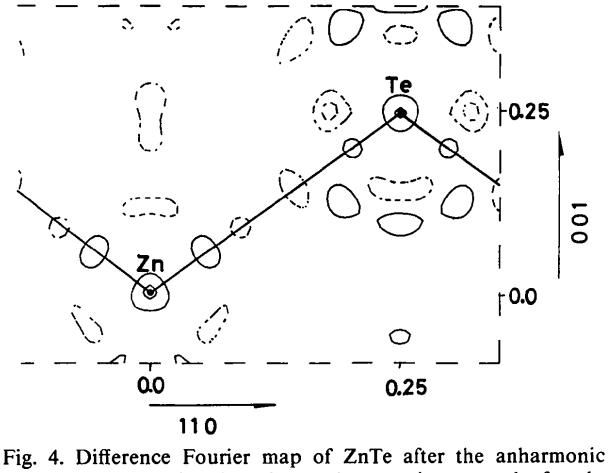

Fig. 4. Difference Fourier map of ZnTe after the anharmonic refinement applying the Edgeworth expansion up to the fourth-order tensor. The Fourier section and contour interval are as in Fig. 1.

Table 5. *OPP parameters of* Zn *and X atoms* ($\times 10^{20}$ J)

	ZnS	ZnSe	ZnTe
$\alpha(\mathrm{Zn})_h$ (Å^{-2})	1·826	1·432	1·228
$\alpha(X)_h$ (Å^{-2})	2·259	2·115	1·756
$\alpha(\mathrm{Zn})$ (Å^{-2})	1·896	1·548	1·246
$\beta(\mathrm{Zn})$ (Å^{-3})	−0·211	−0·383	−0·343
$\gamma(\mathrm{Zn})$ (Å^{-4})	−0·0085	−0·0153	−0·0011
$\delta(\mathrm{Zn})$ (Å^{-4})	0·0056	0·0076	−0·0168
$\alpha(X)$ (Å^{-2})	2·105	2·000	1·557
$\beta(X)$ (Å^{-3})	0·232	0·559	0·464
$\gamma(X)$ (Å^{-4})	0·0411	0·0580	0·0285
$\delta(X)$ (Å^{-4})	0·0121	−0·0325	−0·0522

The one-particle potentials of the three samples ZnX (X = S, Se, Te) along the $[\bar{1}\bar{1}\bar{1}]$ direction of the Zn–X bond and the opposite direction [111] are plotted in terms of the distance u from the Zn position (0, 0, 0) for the three compounds (Fig. 5). The potential curve of ZnTe deviates from the parabolic harmonic potential curve to a larger extent and is located lower than those of the other two compounds. These features interpret well the aforementioned result that ZnTe with the smallest effective charge and force constant shows the most salient anharmonicity of the atomic thermal vibration among the three materials.

The OPP curves of ZnTe in the directions from the Zn position to the nearest Zn atom parallel to [110] and to the second nearest one parallel to [100], besides the bonding direction of $[\bar{1}\bar{1}\bar{1}]$, are plotted in Fig. 6. The OPP curve along [111] is located lower than the other two curves, while that along $[\bar{1}\bar{1}\bar{1}]$ is higher. The

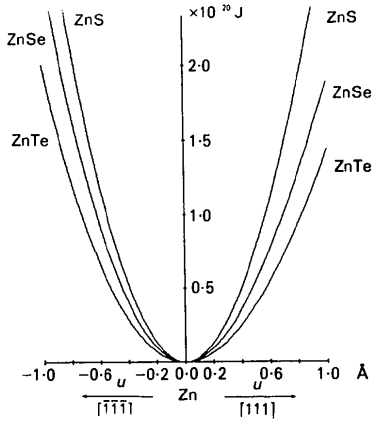

Fig. 5. Effective one-particle potentials of ZnX(X=S, Se, Te) along the directions [111] and $[\bar{1}\bar{1}\bar{1}]$. The abscissa indicates the atomic displacement u from the Zn-atom position (0, 0, 0).

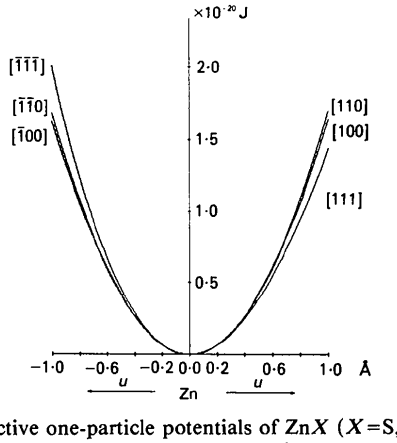

Fig. 6. Effective one-particle potentials of ZnX (X=S, Se, Te) in terms of the atomic displacement u, showing the potential curves along the [111], [110] and [100] directions.

potential curves along [110] and [$\bar{1}\bar{1}$0] and those along [100] and [$\bar{1}$00] are both symmetric with respect to the Zn position, indicating no anisotropic anharmonic features. The curves of the former two potentials are slightly lower than those of the latter.

The potential curves interpret the residual electron densities observed in the difference Fourier map (Fig. 1). The positions of the positive peaks coincide with the smaller potential region, and those of the negative one with the larger potential.

In comparison with the neutron diffraction studies, the present experiment on the anharmonic thermal vibration of atoms in ZnX (X = S, Se, Te) encounters greater difficulty regarding the separation from the valence charge electron distribution mainly observed around the X atoms. However, it is confirmed by the difference Fourier synthesis that the difficulty is overcome by the refinement using the higher-order reflections. The cumulant expansion up to the fourth-rank tensors was adopted for the thermal parameters in the present anharmonic refinements.

The residual electron densities observed in the difference Fourier maps after the harmonic refinements indicate that ZnTe shows more notable anharmonicity than ZnS and ZnSe, and that the Zn atom in the three compounds shows a larger anharmonicity than X. These features are also disclosed by the OPP calculated from the anharmonic parameters.

The lattice-dynamical study by means of Raman spectroscopy elucidates that the compounds having the less ionic but probably more metallic bond character show a larger anharmonicity than the ionic compounds and that the bond distance of the former more easily expands, as the interatomic forces are weakened.

References

BECKER, P. J. & COPPENS, P. (1974). *Acta Cryst.* A**30**, 129-147.
BUSING, W. R. & LEVY, H. A. (1967). *Acta Cryst.* **22**, 457-464.
COHEN, M. L. (1973). *Science*, **179**, 1189-1195.
COOPER, M. J., ROUSE, K. & FUESS, H. (1973). *Acta Cryst.* A**29**, 49-56.
COWLEY, R. A. (1963). *Adv. Phys.* **12**, 421-480.
DICK, B. J. & OVERHAUSER, A. W. (1958). *Phys. Rev.* **112**, 90-103
FINGER, L. W. & PRINCE, E. (1975). *Natl Bur. Stand (US) Tech. Note* No. 854.
JOHNSON, C. K. (1969). *Acta Cryst.* A**25**, 187-194.
JOHNSON, C. K. & LEVY, H. A. (1974). *International Tables for X-ray Crystallography*, Vol. IV, pp. 311-336. Birmingham; Kynoch Press. (Present distributor D. Reidel, Dordrecht.)
KELLERMANN, E. W. (1940). *Philos. Trans. R. Soc. London*, **238**, 513-548.
KONTIO, A. & STEVENS, E. D. (1982). *Acta Cryst.* A**38**, 623-629.
KUHS, W. F. (1983). *Acta Cryst.* A**39**, 148-158.
KUSKOV, V. I., RUSAKOV, A. P. & MENTSER, A. N. (1972). *Sov. Phys. Solid State*, **14**, 1869-1870.
LEE, B. H. (1970). *J. Appl. Phys.* **41**, 2984-2990.
MCINTYRE, C. J., MOSS, G. & BARNEA, Z. (1980). *Acta Cryst.* A**36**, 482-490.
MAIR, S. L. & WILKINS, S. W. (1976). *J. Phys. C*, **9**, 1145-1158.
MERISALO, M. & KURITTU, J. (1978). *J. Appl. Cryst.* **11**, 179-182.
MOSS, B., MCMULLAN, R. K. & KOETZLE, T. F. (1980). *J. Chem. Phys.* **73**, 495-508.
VEKILOV, YU. KH. & RUSAKOV, A. P. (1971). *Sov. Phys. Solid State*, **13**, 956-960.
WILKINSON, G. R. (1973). *The Raman Effect*, Vol. II, edited by A. ANDERSON, pp. 811-987. New York: Academic Press.
WILLIS, B. T. M. (1969). *Acta Cryst.* A**25**, 277-300.
YAMANAKA, T. (1985). *Phys. Chem. Miner.* In preparation.
YAMANAKA, T., TAKEUCHI, Y. & TOKONAMI, M. (1984). *Acta Cryst.* B**40**, 96-102.
ZUCKER, U. H. & SCHULZ, H. (1982). *Acta Cryst.* A**38**, 563-568.

Acta Cryst. (1985). B**41**, 304-310

A Systematic Classification of Crystal Structures

BY LUDO K. FREVEL

Department of Chemistry, The Johns Hopkins University, Baltimore, Maryland 21218, *USA*

(*Received* 19 *March* 1984; *accepted* 7 *May* 1985)

Abstract

A concise scientific notation has been devised to classify the crystal structure of a stoichiometric compound expressed by the formula $\sum_E E_{\nu_E}$, where E represents the chemical symbol of element E and ν_E denotes the number of atoms of element E. Four items of information are coded in the composite notation: (a) the number of different elements, n_E, contained in the chemical formula; (b) the total number of atoms given by the chemical formula; (c) the applicable space group, S, expressed in the Hermann-Maugin notation; and (d) the number of formula 'molecules', z, per unit cell. The general form of any crystal structure is thus expressed as n_E, $\sum_E \nu_E S(z)$. For each crystal system its various crystal structures are catalogued in a hierarchical order so that the structure with the lowest values for n_E, $\sum \nu_E$, z and the lowest space-group number is listed first. The crystal structure 1,1P1(1) heads the list of triclinic structures. A simple augmentation of the proposed notation makes it possible to classify also the non-stoichiometric defect structures.

0108-7681/85/050304-07$01.50